



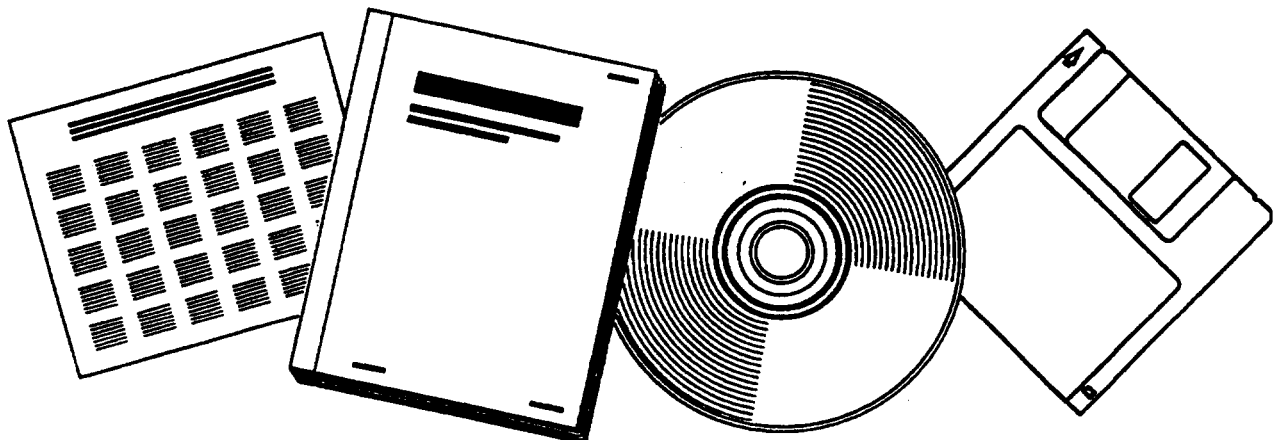
DE91014240

NTIS
Information Is Our Business.

HYDRODYNAMICS OF THE THREE-PHASE SLURRY FISCHER-TROPSCH BUBBLE COLUMN REACTORS. FINAL REPORT

TEXAS A AND M UNIV., COLLEGE STATION.
DEPT. OF CHEMICAL ENGINEERING

SEP 1990



U.S. DEPARTMENT OF COMMERCE
National Technical Information Service

DE91-014240



DOE/PC/90012-10
(DE91014240)

Energy

F
O
S
S
I
L

HYDRODYNAMICS OF THREE-PHASE SLURRY FISCHER-TROPSCH BUBBLE
COLUMN REACTORS

Final Report

By
Dragomir B. Bukur
James G. Daly
Snehal A. Patel

September 1990

Work Performed Under Contract No. AC22-86PC90012

For
U.S. Department of Energy
Pittsburgh Energy Technology Center
Pittsburgh, Pennsylvania

By
Texas A&M University
College Station, Texas

REPRODUCED BY
U.S. DEPARTMENT OF COMMERCE
NATIONAL TECHNICAL
INFORMATION SERVICE
SPRINGFIELD, VA 22161

HYDRODYNAMICS OF THREE-PHASE SLURRY
FISCHER-TROPSCH BUBBLE COLUMN REACTORS

FINAL REPORT

DRAGOMIR B. BUKUR, JAMES G. DALY AND SNEHAL A. PATEL

TEXAS A&M UNIVERSITY
DEPARTMENT OF CHEMICAL ENGINEERING
COLLEGE STATION, TX 77843

September 1990

Prepared for the Pittsburgh Energy Technology Center,
the United States Department of Energy Under Contract No. DE-AC22-86PC90012
George Cinquegrane, Project Manager (PETC)
John Shen, Program Manager (DOE/FE)

TABLE OF CONTENTS

	Page
LIST OF TABLES	vi
LIST OF FIGURES	x
ABSTRACT	xix
OBJECTIVES AND SCOPE OF WORK	xx
EXECUTIVE SUMMARY	xxii
RECOMMENDATIONS FOR FUTURE WORK	xxviii
I. INTRODUCTION	1
Overview of Fischer-Tropsch Studies in Bubble Columns	3
Mass transfer coefficient	5
Heat transfer coefficient	6
Gas holdup and bubble size distribution	6
Flow regime characterization	10
Effect of solids	10
Effect of liquid velocity	11
Overview of Nuclear Density Gauge Studies	12
Objectives of This Study	16
II. MEASUREMENT OF GAS HOLDUPS BY CONVENTIONAL TECHNIQUES	17
Experimental Apparatus and Operating Procedure	17
Experimental Conditions	29
Data Acquisition and Reduction Procedures for Gas Holdups and Solids Concentration Profiles	29
Average gas holdup - glass columns	32
Phase fractions - stainless steel columns	32
Pressure measurements	32
Solid concentration measurements	36
Holdup calculations	42
Results and Discussion	47
Description of the flow field	47

	Page
Gas holdup results	49
Effect of slurry velocity	51
Effect of solids concentration	62
Effect of solids type and size	77
Effect of liquid medium	82
Effect of distributor type	85
Effect of column diameter	87
Physical Properties and Average Gas Holdup Correlations	92
Physical property measurements	92
Density measurements	92
Viscosity measurements	94
Surface tension measurements	95
Gas holdup correlations	97
III. MEASUREMENT OF PHASE FRACTIONS BY GAMMA-RAY DENSITOMETRY	111
Theoretical Discussion	111
Models used to describe three-phase systems	115
Case I. Perpendicular alignment	115
Case II. Parallel alignment	119
Comments on the alignment of the phases	122
Source Selection and Sensitivity Analysis	123
Experimental Apparatus and Operating Conditions	130
Movable assembly mechanism (MAM)	130
Sources and detectors	133
Nuclear electronics	135
Calibration procedures	141
Data Acquisition and Reduction Procedures	143
Gas holdups in two-phase systems	147
Gas holdups in three-phase systems	154
Discussion of Results	154
Independent treatment of all three phases	155
Two-phase and pseudo two-phase results	157

	Page
IV. AXIAL SOLIDS DISTRIBUTION	184
Semi-Infinite Dispersion Model	184
Summary of Solids Concentrations in the Column and Storage Tank	188
Results and Discussion	193
V. BUBBLE SIZE DISTRIBUTIONS	211
Experimental Techniques for Measurement of the Disengagement Profile	215
Theory	216
Case I. Constant rate disengagement process	217
Estimating bubble rise velocities and gas holdups during constant rate disengagement	223
Estimating bubble diameters and specific gas-liquid interfacial area	223
Data Acquisition and Reduction Procedures	228
Discussion of Results	231
Effect of axial position	247
Effect of column diameter	249
Comparison of results obtained in the glass and stainless steel bubble columns	251
VI. FLOW REGIME CHARACTERIZATION	256
Theoretical Background	256
Discussion of Results	262
Flow regime transitions based on the MSE	268
Flow regime transitions based on the PSD	279
VII. NOMENCLATURE	294
VIII. LITERATURE CITED	300
IX. ACKNOWLEDGMENTS	311

LIST OF TABLES

Table	Page
1.1. Summary of Bubble Column Hydrodynamic Studies	4
1.2. Summary of Nuclear Density Gauge Studies.	14
2.1. Bubble Column Dimensions and Experimental Conditions	28
2.2a. Results from Archimedean Procedure (0-5 μm iron oxide in FT-300)	40
2.2b. Results from Archimedean Procedure (20-44 μm iron oxide in FT-300)	40
2.2c. Results from Archimedean Procedure (0-5 μm silica in FT-300)	40
2.3a. Results from Archimedean Procedure (0-5 μm iron oxide in SASOL)	41
2.3b. Results from Archimedean Procedure (20-44 μm silica in SASOL)	41
2.4. Summary of Runs in the Small Stainless Steel Column	50
2.5. Summary of Runs in the Large Stainless Steel Column	52
2.6. Physical Properties of FT-300 Wax and SASOL Wax	93
2.7. Summary of Gas Holdup Correlations Presented in the Literature	98
2.8. Summary of Number of Points at a Given Set of Conditions	102
2.9. Mean Square Errors for Literature Correlations	104
2.10. Goodness of Fit and Parameters for Empirical Holdup Correlation	107
3.1. Attenuation Coefficients (cm^{-1}) Used for Error Analysis Calculations	128
3.2a. Effect of Errors in the Count Rate of Co-60 on Volume Fractions Using the Am-241 and Co-60 System	128
3.2b. Effect of Errors in the Count Rate of Am-241 on Volume Fractions Using the Am-241 and Co-60 System	128
3.3a. Effect of Errors in the Count Rate of Co-60 on Volume Fractions Using the Cs-137 and Co-60 System	129
3.3b. Effect of Errors in the Count Rate of Cs-137 on Volume Fractions Using the Cs-137 and Co-60 System	129
3.4. Summary of Nuclear Density Gauge Electronics	139
3.5. Summary of Settings for the High Voltage Supply (HVS), Amplifier (AMP), and Single Channel Analyzer (SCA)	139

Table	Page
3.6. Measured Attenuation Coefficients (cm^{-1}) for FT-300 wax, SASOL wax, Iron Oxide, and Silica	144
3.7. Comparison of Measured and Theoretical Attenuation Coefficients (cm^{-1})	144
3.8. Distance Through the Column for Both Sources at All Locations for the Experiments with FT-300 Wax	148
3.9a. Effect of Technique Used to Obtain Average Gas Holdups from Axial Gas Holdups (Data from Experiment 4 in Table 2.7, $u_g=0.02 \text{ m/s}$)	153
3.9b. Effect of Technique Used to Obtain Average Gas Holdups from Axial Gas Holdups (Data from Experiment 4 in Table 2.7, $u_g=0.09 \text{ m/s}$)	153
3.10a. Gas Holdups from Measurements with the Nuclear Density Gauge at a Height of 1.5 m Above the Distributor (FT-300 Wax, 20 wt% 20-44 μm Iron Oxide)	156
3.10b. Gas and Solids Holdups from Measurements with the Nuclear Density Gauge at a Height of 1.5 m Above the Distributor After Modifying the Thickness (d) of the Absorbing Media (FT-300 Wax, 20 wt% 20-44 μm Iron Oxide)	156
3.11a. Gas Holdups from Measurements with the Nuclear Density Gauge at a Height of 1.5 m Above the Distributor (SASOL Wax, 20 wt% 20-44 μm Silica)	158
3.11b. Gas and Solids Holdups from Measurements with the Nuclear Density Gauge at a Height of 1.5 m Above the Distributor After Modifying the Thickness (d) of the Absorbing Media (SASOL Wax, 20 wt% 20-44 μm Silica)	158
3.12a. Gas Holdups from Measurements with the Nuclear Density Gauge at a Height of 2.1 m Above the Distributor (FT-300 Wax, 20 wt% 20-44 μm Iron Oxide)	159
3.12b. Gas and Solids Holdups from Measurements with the Nuclear Density Gauge at a Height of 2.1 m Above the Distributor After Modifying the Thickness (d) of the Absorbing Media (FT-300 Wax, 20 wt% 20-44 μm Iron Oxide)	159
3.13a. Gas Holdups from Measurements with the Nuclear Density Gauge at a Height of 0.9 m Above the Distributor (SASOL Wax, 20 wt% 20-44 μm Silica)	160

Table	Page
3.13b. Gas and Solids Holdups from Measurements with the Nuclear Density Gauge at a Height of 0.9 m Above the Distributor After Modifying the Thickness (d) of the Absorbing Media (SASOL Wax, 20 wt% 20-44 μm Silica)	160
3.14a. Gas Holdups from Measurements with the Nuclear Density Gauge at a Height of 1.5 m Above the Distributor (SASOL Wax, 20 wt% 0-5 μm Iron Oxide)	161
3.14b. Gas and Solids Holdups from Measurements with the Nuclear Density Gauge at a Height of 1.5 m Above the Distributor After Modifying the Thickness (d) of the Absorbing Media (SASOL Wax, 20 wt% 0-5 μm Iron Oxide)	161
3.15a. Radial Gas Holdups Obtained Using the Co-60 Source (SASOL Wax, No Solids, $u_{sl}=0$ m/s)	167
3.15b. Radial Gas Holdups Obtained Using the Cs-137 Source (SASOL Wax, No Solids, $u_{sl}=0$ m/s)	167
3.16a. Radial Gas Holdups Obtained Using the Co-60 Source (SASOL Wax, 20 wt% 0-5 μm Iron Oxide, $u_{sl}=0.005$ m/s)	168
3.16b. Radial Gas Holdups Obtained Using the Cs-137 Source (SASOL Wax, 20 wt% 0-5 μm Iron Oxide, $u_{sl}=0.005$ m/s)	168
3.17a. Radial Gas Holdups Obtained Using the Co-60 Source (SASOL Wax, 20 wt% 20-44 μm Silica, $u_{sl}=0$ m/s)	169
3.17b. Radial Gas Holdups Obtained Using the Cs-137 Source (SASOL Wax, 20 wt% 20-44 μm Silica, $u_{sl}=0$ m/s)	169
3.18a. Radial Gas Holdups Obtained Using the Co-60 Source (FT-300 Wax, 20 wt% 20-44 μm Iron Oxide, $u_{sl}=0$ m/s)	170
3.18b. Radial Gas Holdups Obtained Using the Cs-137 Source (FT-300 Wax, 20 wt% 20-44 μm Iron Oxide, $u_{sl}=0$ m/s)	170
4.1a. Summary of Solids Concentrations For Experiments in the 0.05 m ID Bubble Column	190
4.1b. Summary of Solids Concentrations For Experiments in the 0.21 m ID Bubble Column	191
5.1. Correlations for Estimating Bubble Size from Bubble Rise Velocity	226

Table	Page
5.2a. DGD Results from the Experiment with FT-300 Wax at a Height of 1.3 m (0.21 m ID Stainless Steel Bubble Column, 265 °C)	235
5.2b. DGD Results from the Experiment with FT-300 Wax at a Height of 1.9 m (0.21 m ID Stainless Steel Bubble Column, 265 °C)	235
5.3a. DGD Results from the Experiment with SASOL Wax (Decreasing Gas Velocity) at a Height of 1.3 m (0.21 m ID Stainless Steel Bubble Column, 265 °C)	236
5.3b. DGD Results from the Experiment with SASOL Wax (Decreasing Gas Velocity) at a Height of 1.9 m (0.21 m ID Stainless Steel Bubble Column, 265 °C)	236
5.4a. DGD Results from the Experiment with SASOL Wax (Increasing Gas Velocity) at a Height of 1.3 m (0.21 m ID Stainless Steel Bubble Column, 265 °C)	237
5.4b. DGD Results from the Experiment with SASOL Wax (Increasing Gas Velocity) at a Height of 1.9 m (0.21 m ID Stainless Steel Bubble Column, 265 °C)	237
5.5a. DGD Results from the Experiment with FT-300 Wax (Increasing Gas Velocity) at a Height of 1.3 m (0.05 m ID Stainless Steel Bubble Column, 265 °C)	239
5.5b. DGD Results from the Experiment with SASOL Wax (Increasing Gas Velocity) at a Height of 1.9 m (0.05 m ID Stainless Steel Bubble Column, 265 °C)	239
5.6a. DGD Results from the Experiment with SASOL Wax (Increasing Gas Velocity) at a Height of 1.3 m (0.05 m ID Stainless Steel Bubble Column, 265 °C)	240
5.6b. DGD Results from the Experiment with SASOL Wax (Increasing Gas Velocity) at a Height of 1.9 m (0.05 m ID Stainless Steel Bubble Column, 265 °C)	240

LIST OF FIGURES

Figure	Page
2.1. Schematic of the slurry bubble column apparatus.	18
2.2. Schematic representation of the slurry inlet system for the large diameter stainless steel column.	20
2.3. Schematic representation of the slurry inlet system for the small diameter stainless steel column.	21
2.4. Schematic representation of the circulation loop for the large diameter stainless steel column.	24
2.5. Schematic representation of the circulation loop for the small diameter stainless steel column.	25
2.6. Schematic representation of the dipstick assembly.	26
2.7. Schematic representation of the perforated plate distributor.	30
2.8. Schematic representation of the bubble cap distributor plate.	31
2.9. Schematic diagram of the pressure ports and slurry sampling ports locations (all dimensions in m).	33
2.10. Schematic representation of the pressure transducer system.	34
2.11. Typical pressure transducer calibration curve.	37
2.12. Bubble column flow regime map (adopted from Deckwer et al., 1980).	48
2.13. Effect of superficial slurry velocity on average gas holdup in the (a) small and (b) large diameter columns with FT-300 wax.	53
2.14. Effect of superficial gas velocity on axial gas holdup in the (a) small and (b) large diameter columns with FT-300 wax.	55
2.15. Effect of superficial slurry velocity on axial gas holdup in the small diameter column with FT-300 wax.	57
2.16. Effect of superficial slurry velocity on average gas holdup in the small diameter column with FT-300 wax in the presence of solids; (a) 0–5 μm iron oxide; (b) 0–5 μm silica.	59
2.17. Effect of superficial slurry velocity on average gas holdup in the large diameter column with FT-300 wax (20–44 μm iron oxide).	60

Figure	Page
2.18. Effect of superficial slurry velocity on average gas holdup in the (a) small and (b) large diameter columns with SASOL wax.	61
2.19. Effect of slurry velocity on average gas holdup in the large diameter column with SASOL wax ((a) 0–5 μm iron oxide, (b) 20–44 μm iron oxide, (c) 20–44 μm silica).	63
2.20. Effect of solids concentration on average gas holdup with FT-300 wax ((a) 0.05 m ID Column, 20 WT%, 0–5 μm iron oxide; (b) 0.21 m ID Column, 20 WT%, 20–44 μm iron oxide).	64
2.21. Effect of solids concentration and superficial gas velocity on axial gas holdup in the 0.05 m ID column with FT-300 wax (0–5 μm iron oxide particles; (a) $u_g = 0.02 \text{ m/s}$; (b) $u_g = 0.04 \text{ m/s}$; (c) $u_g = 0.12 \text{ m/s}$).	66
2.22. Effect of solids concentration on average gas holdup in the 0.05 m ID column with FT-300 wax ((a) 20–44 μm iron oxide; (b) 0–5 μm silica).	67
2.23. Effect of solids concentration on average gas holdup neglecting foam (0–5 μm iron oxide).	70
2.24. Effect of solids concentration on average gas holdup in the continuous mode of operation with FT-300 wax (0–5 μm iron oxide; (a) $u_{sl} = 0.005 \text{ m/s}$; (b) $u_{sl} = 0.02 \text{ m/s}$).	72
2.25. Effect of solids concentration on average gas holdup with FT-300 wax ((a) 0.05 m ID column, 0–5 μm silica; (b) 0.21 m ID column, 20–44 μm iron oxide).	73
2.26. Effect of solids concentration on average gas holdup with SASOL wax ((a) 0.05 m ID column, 20–44 μm iron oxide, (b) 0.21 m ID column, 20–44 μm iron oxide, (c) 0.21 m ID column, 0–5 μm iron oxide).	74
2.27. Effect of solids concentration on average gas holdup with SASOL wax in the continuous mode of operation ((a) 0.05 m ID column, 20–44 μm iron oxide, (b) 0.21 m ID column, 20–44 μm iron oxide, (c) 0.21 m ID column, 0–5 μm iron oxide).	76
2.28. Effect of solids type and size on average gas holdup in the 0.05 m ID column with FT-300 wax.	78

Figure

Page

2.29. Effect of solids type and size on average gas holdup in the 0.05 m ID column with FT-300 wax (volume fraction of solids at the distributor = 0.045).	80
2.30. Effect of solids type and size on average gas holdup in the 0.21 m ID column with SASOL wax ((a) $u_{sl} = 0.0 \text{ m/s}$; (b) $u_{sl} = 0.005 \text{ m/s}$).	81
2.31. Effect of liquid medium on average gas holdup in the 0.05 m ID column.	83
2.32. Effect of liquid medium on average gas holdup in the 0.21 m ID column.	84
2.33. Effect of superficial gas velocity and distributor type on average gas holdup (20 - 44 μm iron oxide; (a) SASOL wax, $u_{sl} = 0.0 \text{ m/s}$; (b) FT-300 wax, $u_{sl} = 0.005 \text{ m/s}$).	86
2.34. Effect of superficial gas velocity and distributor type on average gas holdup with SASOL wax (0 - 5 μm iron oxide; (a) $u_{sl} = 0.0 \text{ m/s}$; (b) $u_{sl} = 0.005 \text{ m/s}$).	88
2.35. Effect of column diameter on average gas holdup with FT-300 wax.	89
2.36. Effect of column diameter on average gas holdup with SASOL wax.	91
2.37. Effect of temperature on surface tension of fresh and used FT-300 and SASOL wax.	96
2.38. Parity plot of predicted versus measured gas holdup ((a and b) Badjugar et al., 1986; (c and d) Hughmark, 1967).	105
2.39. Parity plot of predicted versus measured gas holdups for the correlations developed in this study.	108
2.40. Parity plot of predicted versus measured gas holdup (wax type: SASOL, FT-300, Mobil; $u_g = 0.01$ to 0.15 m/s ; $u_{sl} = 0, 0.005$, and 0.02 m/s ; $d_c = 0.05$ and 0.21 m ID; solids: 0, 10, 20, and 30 wt% iron oxide and silica).	110
3.1. Relative importance of the three major types of gamma-ray attenuation.	114
3.2. Schematic representation of multiple absorbers in series.	116

Figure	Page
3.3. Schematic representation of Case I geometry (i.e. perpendicular alignment)	118
3.4. Schematic representation of Case II geometry (i.e. parallel alignment).	120
3.5. Schematic representations of (a) annular flow and (b) homogeneous flow in a square duct.	124
3.6. Schematic diagram of axial movement mechanism for the nuclear density gauge apparatus	131
3.7. Schematic diagram of the radial movement mechanism for the nuclear density gauge apparatus	132
3.8. Schematic representation of the Cobalt-60 source holder.	136
3.9. Schematic representation of the Cesium-137 source holder.	137
3.10. Schematic representation of the detector housing for the Cobalt-60 and Cesium-137 sources.	138
3.11. Schematic diagram of the nuclear density gauge electronic and data acquisition system.	140
3.12. Schematic diagram of the calibration chamber.	142
3.13. Schematic diagram of the nuclear density gauge measurement locations.	146
3.14. Schematic representation of the locations for radial measurements with the nuclear density gauge apparatus.	149
3.15. Schematic diagram of the regions used to obtain average gas holdups.	152
3.16. Effect of superficial gas velocity on radial gas holdup (SASOL wax, no solids, $u_{sl} = 0.0 \text{ m/s}$).	162
3.17. Effect of superficial gas velocity on radial gas holdup (SASOL wax, 20 wt% 0 - 5 μm iron oxide, $u_{sl} = 0.005 \text{ m/s}$).	163
3.18. Effect of superficial gas velocity on radial gas holdup (SASOL wax, 20 wt% 20 - 44 μm silica, $u_{sl} = 0.0 \text{ m/s}$).	164
3.19. Effect of superficial gas velocity on radial gas holdup (FT-300 wax, 20 wt% 20 - 44 μm iron oxide, $u_{sl} = 0.0 \text{ m/s}$).	165
3.20. Schematic representation of bubble column wall.	171

Figure	Page
3.21. Comparison of average gas holdups from the DP cells and nuclear density gauges (SASOL wax, no solids; (a) $u_\ell = 0.0 \text{ m/s}$, (b) $u_\ell = 0.005 \text{ m/s}$).	173
3.22. Comparison of average gas holdups from the DP cells and nuclear density gauges (SASOL wax, 20 wt% 0 - 5 μm iron oxide; (a) $u_{sl} = 0.0 \text{ m/s}$; (b) $u_{sl} = 0.005 \text{ m/s}$; (c) $u_{sl} = 0.02 \text{ m/s}$).	174
3.23. Comparison of axial gas holdups from the DP cells and nuclear density gauges (SASOL wax, no solids; (a) $u_g = 0.04 \text{ m/s}$; (b) $u_g = 0.09 \text{ m/s}$).	176
3.24. Comparison of average gas holdups from the DP cells and nuclear density gauges (SASOL wax, $u_{sl} = 0.0 \text{ m/s}$; (a) 20 wt% 20-44 μm iron oxide; (b) 20 wt% 20-44 μm silica).	177
3.25. Comparison of axial gas holdups from the DP cells and nuclear density gauges (SASOL wax, 20 wt% 20-44 μm iron oxide - (a) $u_g = 0.02 \text{ m/s}$; (b) $u_g = 0.08 \text{ m/s}$; SASOL wax, 20 wt% 20-44 μm silica - (c) $u_g = 0.02 \text{ m/s}$; (d) $u_g = 0.08 \text{ m/s}$).	178
3.26. Comparison of average gas holdups from the DP cells and nuclear density gauges (FT-300 wax; (a) $u_\ell = 0.0 \text{ m/s}$, no solids; (b) $u_\ell = 0.005 \text{ m/s}$, no solids; (c) $u_{sl} = 0.0 \text{ m/s}$, 20 wt% 20-44 μm iron oxide).	180
3.27. Comparison of axial gas holdups from the DP cells and nuclear density gauges with FT-300 wax and no solids ($u_\ell = 0.0 \text{ m/s}$ (a) $u_g = 0.04 \text{ m/s}$; (b) $u_g = 0.12 \text{ m/s}$; $u_\ell = 0.005 \text{ m/s}$ - (c) $u_g = 0.04 \text{ m/s}$; (d) $u_g = 0.12 \text{ m/s}$).	181
3.28. Comparison of axial gas holdups from the DP cells and nuclear density gauges (FT-300 wax, 20 wt% 20-44 μm iron oxide - (a) $u_g = 0.02 \text{ m/s}$; (b) $u_g = 0.04 \text{ m/s}$; (c) $u_g = 0.08 \text{ m/s}$).	183
4.1. Schematic diagram of modified expansion unit.	192
4.2. Effect of axial position and superficial gas velocity on solids concentrations (0-5 μm particles, $u_{sl} = 0.0 \text{ m/s}$; (a) iron oxide, 0.05 m ID column; (b) silica, 0.05 m ID column; (c) iron oxide, 0.21 m ID column).	195
4.3. Effect of axial position and superficial gas velocity on solids concentrations (20-44 μm particles, 0.05 m ID bubble column; (a) iron oxide, $u_{sl} = 0 \text{ m/s}$; (b) silica, $u_{sl} = 0 \text{ m/s}$; (c) iron oxide, $u_{sl} = 0.02 \text{ m/s}$).	196

Figure	Page
4.4. Effect of axial position and superficial gas velocity on solids concentrations (20 wt% 20-44 μm iron oxide particles, 0.21 m ID bubble column, $u_{sl}=0$ m/s; (a) 19 x 2 mm PP distributor; (b) bubble cap distributor).	197
4.5. Effect of axial position and superficial gas velocity on solids concentrations (20-44 μm iron oxide particles, 0.21 m ID bubble column, $u_{sl}=0.005$ m/s; (a) 30 wt%; (b) 20 wt%).	199
4.6. Effect of superficial gas velocity on u_p/E_s (20-44 μm particles, $u_{sl}=0.0$ m/s; (a) iron oxide, 0.05 m ID column; (b) silica, 0.05 m ID column; (c) iron oxide, 0.21 m ID column).	201
4.7. Effect of superficial gas velocity on hindered particle settling velocity for 20-44 μm iron oxide particles in SASOL reactor wax.	202
4.8. Effect of superficial gas velocity on axial solids dispersion coefficients ((a) 0.05 m ID column, (b) 0.21 m ID column).	204
4.9. Parity plot of measured versus predicted solids concentrations; (20-44 μm iron oxide and silica particles; $u_{sl}=0.0$ m/s and 0.005 m/s-0.21 m ID column only).	205
4.10. Effect of superficial gas velocity on axial solids concentrations (0-5 μm particles; 0.05 m ID bubble column; $u_{sl}=0$ m/s; (a) iron oxide; (b) silica).	207
4.11. Effect of particle size and superficial gas velocity on axial solids concentrations.	208
4.12. Effect of column diameter and superficial slurry velocity on axial solids concentrations.	210
5.1. Dispersion prior to disengagement ($t = 0$).	218
5.2. Dispersion during the constant rate disengagement process (Period 1).	219
5.3. Dispersion during the constant rate disengagement process (Period 2).	222
5.4. Plot of height vs. time for a multimodal distribution (constant rate process).	224
5.5. Bubble rise velocity vs. bubble diameter correlation for FT-300 wax.	227

Figure	Page
5.6. Raw pressure transducer signal for DGD analysis from the experiment with FT-300 wax in the small diameter column at heights of (a) 0.6 m; (b) 1.3 m; and (c) 1.9 m above the distributor.	230
5.7. Effect of axial position on disengagement (FT-300 wax, (a) $u_g = 0.02 \text{ m/s}$; (b) $u_g = 0.12 \text{ m/s}$)	232
5.8. Effect of axial position on disengagement (SASOL wax, (a) $u_g = 0.02 \text{ m/s}$; (b) $u_g = 0.09 \text{ m/s}$)	233
5.9. Effect of superficial gas velocity and wax type on (a) Sauter mean bubble diameter, (b) specific gas-liquid interfacial area, and (c) gas holdup in the 0.21 m ID column at a height of 1.3 m above the distributor.	241
5.10. Effect of superficial gas velocity and wax type on (a) Sauter mean bubble diameter, (b) specific gas-liquid interfacial area, and (c) gas holdup in the 0.21 m ID column at a height of 1.9 m above the distributor.	243
5.11. Effect of superficial gas velocity and wax type on (a) Sauter mean bubble diameter, (b) specific gas-liquid interfacial area, and (c) gas holdup in the 0.05 m ID column at a height of 1.3 m above the distributor.	244
5.12. Effect of superficial gas velocity and wax type on (a) Sauter mean bubble diameter, (b) specific gas-liquid interfacial area, and (c) gas holdup in the 0.05 m ID column at a height of 1.9 m above the distributor.	245
5.13. Effect of superficial gas velocity on axial gas holdup ((a) 0.05 m ID column, FT-300 wax; (b) 0.05 m ID column, SASOL wax; (c) 0.21 m ID column, FT-300 wax).	246
5.14. Effect of axial position on (a and c) Sauter mean bubble diameter and (b and d) gas holdup in 0.05 and 0.21 m ID bubble columns with wax (decreasing gas velocity - SASOL wax, 0.21 m ID column).	248
5.15. Effect of column diameter on Sauter mean bubble diameter for (a) FT-300 wax and (b) SASOL reactor wax - decreasing gas velocity in 0.21 m ID column.	250
5.16. Comparison of (a) Sauter mean bubble diameters and (b) gas holdup obtained in the 0.21 m ID stainless steel column (DP method, 1.9 m) and the 0.23 m ID glass column (visual method) with FT-300 wax.	252

Figure	Page
5.17. Comparison of (a) Sauter mean bubble diameters and (b) gas holdup obtained in the 0.05 m ID stainless steel column (DP method, 1.9 m) and the 0.05 m ID glass column (visual method) with FT-300 wax.	253
5.18. Comparison of (a) Sauter mean bubble diameters and (b) gas holdup obtained in the 0.05 m ID stainless steel column (DP method, 1.9 m) and the 0.05 m ID glass column (visual method) with SASOL wax.	255
6.1. Typical raw signals from the nuclear density gauge apparatus during experiments in the 0.05 m ID bubble column.	264
6.2. Typical raw signals from the nuclear density gauge apparatus during experiments in the 0.21 m ID bubble column.	265
6.3. Effect of superficial gas velocity on the probability density function from the pressure transducer in the 0.05 m ID bubble column at a height of 1.8 m above the distributor.	266
6.4. Effect of superficial gas velocity on the probability density function from the pressure transducer in the 0.21 m ID bubble column at a height of 1.8 m above the distributor.	267
6.5. Effect of superficial gas velocity on the probability density function from the nuclear density gauge using the Cesium-137 source in the 0.05 m ID bubble column at a height of 1.5 m above the distributor.	269
6.6. Effect of superficial gas velocity on the probability density function from the nuclear density gauge using the Cesium-137 source in the 0.21 m ID bubble column at a height of 1.5 m above the distributor.	270
6.7. Effect of slurry flow rate on the mean square error of pressure fluctuations at the wall (FT-300 wax, 265 °C, 0-5 μm silica, 0.05 m ID column, 1.2 m above the distributor).	272
6.8. Effect of height above the distributor on the mean square error of pressure fluctuations at the wall (FT-300 wax, 265 °C, 20 wt% 0-5 μm silica, 0.05 m ID column, $u_{sl}=0.0$ m/s).	274
6.9. Effect of superficial gas velocity on the mean square error of pressure fluctuations at the wall (FT-300 wax, 265 °C, 20 wt% 0-5 μm silica, 0.05 m ID column, $u_{sl}=0.0$ m/s).	275
6.10. Effect of slurry flow rate and distributor on the mean square error of nuclear density gauge fluctuations (SASOL wax, 265 °C, 0.21 m ID column, Cesium-137 source, 1.5 m above the distributor).	277

Figure	Page
6.11. Effect of height above the distributor on the mean square error of pressure fluctuations at the wall (SASOL wax, 265 °C, 0.21 m ID column, $u_\ell=0.0$ m/s).	278
6.12. Effect of superficial gas velocity on the mean square error of pressure fluctuations at the wall (SASOL wax, 265 °C, 0.21 m ID column, $u_\ell=0.0$ m/s).	280
6.13. Effect of superficial gas velocity on the power spectral density function for pressure fluctuations at the wall (FT-300 wax, 265 °C, 0.05 m ID column, 10 wt% 20-44 μm iron oxide, $u_{sl}=0.02$ m/s, height=1.8 m).	282
6.14. Effect of height above the distributor on the power spectral density function for pressure fluctuations at the wall (FT-300 wax, 265 °C, 0.05 m ID column, 10 wt% 20-44 μm iron oxide, $u_{sl}=0.02$ m/s, $u_g=0.12$ m/s).	283
6.15. Effect of height above the distributor on the power spectral density function for pressure fluctuations at the wall (FT-300 wax, 265 °C, 0.05 m ID column, 20 wt% 0-5 μm silica, $u_{sl}=0.0$ m/s, $u_g=0.09$ m/s).	284
6.16. Effect of superficial gas velocity on the power spectral density function from the nuclear density gauge (FT-300 wax, 265 °C, 0.05 m ID column, $u_\ell=0.0$ m/s, Cesium-137, height=1.5 m).	286
6.17. Effect of superficial gas velocity on the power spectral density function for pressure fluctuations at the wall (SASOL wax, 265 °C, 0.21 m ID column, $u_\ell=0.0$ m/s, height=0.08 m).	288
6.18. Effect of superficial gas velocity on the power spectral density function for pressure fluctuations at the wall (SASOL wax, 265 °C, 0.21 m ID column, $u_\ell=0.0$ m/s, height=1.8 m).	289
6.19. Effect of height above the distributor on the power spectral density function for pressure fluctuations at the wall (SASOL wax, 265 °C, 0.21 m ID column, $u_\ell=0.0$ m/s, $u_g=0.02$ m/s).	290
6.20. Effect of height above the distributor on the power spectral density function for pressure fluctuations at the wall (SASOL wax, 265 °C, 0.21 m ID column, $u_\ell=0.0$ m/s, $u_g=0.06$ m/s).	291
6.21. Effect of height above the distributor on the power spectral density function for nuclear density gauge fluctuations (FT-300 wax, 265 °C, 0.21 m ID column, Cobalt 60, height=1.5 m).	293